

# Catalyst-Free Synthesis of Nitrogen-Doped Graphene *via* Thermal Annealing Graphite Oxide with Melamine and Its Excellent Electrocatalysis

Zhen-Huan Sheng, Lin Shao, Jing-Jing Chen, Wen-Jing Bao, Feng-Bin Wang,\* and Xing-Hua Xia\*

Key Laboratory of Analytical Chemistry for Life Science, School of Chemistry and Chemical Engineering, Nanjing University, Nanjing 210093, China.

Graphene, single-layer carbon atoms densely packed into a two-dimensional honeycomb lattice, is the mother of all graphitic materials such as fullerenes, carbon nanotubes (CNTs), and graphite.<sup>1,2</sup> Owing to the unique properties<sup>3,4</sup> and potential applications of graphene in nanoelectronics,<sup>5–7</sup> energy storage materials,<sup>8–10</sup> polymer composite materials,<sup>11,12</sup> and sensing,<sup>13–15</sup> approaches for the preparation of high-quality graphene in large-scale has been intensively explored in recent years. Besides the original method of micromechanical cleavage of highly oriented pyrolytic graphite (HOPG), efforts have also been made to prepare large-area, high-quality graphene through different kinds of methods, such as chemical vapor deposition (CVD)<sup>16,17</sup> and liquid-phase exfoliation of intercalated graphite compounds.<sup>18</sup> Obviously, the need for the ultimate goal of graphene-based electronic devices and analytical techniques will continue to motivate research in this aspect.

Successful application of graphene in various areas, such as nanoelectronics and biosensing, will be certainly determined by its physical and chemical properties; that is, the electronic properties show considerable effects on the graphene-based devices.<sup>19</sup> Therefore, various strategies have been adopted to tailor the electronic properties of graphene *via* physical and chemical means.<sup>20,21</sup> Both theoretical calculations and detailed experiments have proved that chemical doping with foreign atoms is an effective approach to achieve this goal. For instance, n-type semiconductors can be obtained by replacing carbon atoms with nitrogen atoms in graphene frameworks.<sup>21,22</sup> The lone electron pairs of nitrogen atoms

**ABSTRACT** The electronic and chemical properties of graphene can be modulated by chemical doping foreign atoms and functional moieties. The general approach to the synthesis of nitrogen-doped graphene (NG), such as chemical vapor deposition (CVD) performed in gas phases, requires transitional metal catalysts which could contaminate the resultant products and thus affect their properties. In this paper, we propose a facile, catalyst-free thermal annealing approach for large-scale synthesis of NG using low-cost industrial material melamine as the nitrogen source. This approach can completely avoid the contamination of transition metal catalysts, and thus the intrinsic catalytic performance of pure NGs can be investigated. Detailed X-ray photoelectron spectrum analysis of the resultant products shows that the atomic percentage of nitrogen in doped graphene samples can be adjusted up to 10.1%. Such a high doping level has not been reported previously. High-resolution N1s spectra reveal that the as-made NG mainly contains pyridine-like nitrogen atoms. Electrochemical characterizations clearly demonstrate excellent electrocatalytic activity of NG toward the oxygen reduction reaction (ORR) in alkaline electrolytes, which is independent of nitrogen doping level. The present catalyst-free approach opens up the possibility for the synthesis of NG in gram-scale for electronic devices and cathodic materials for fuel cells and biosensors.

**KEYWORDS:** nitrogen-doped graphene · catalyst-free approach · thermal annealing · melamine · oxygen reduction reaction · electrocatalysis

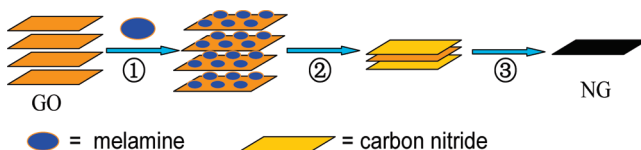
can form a delocalized conjugated system with the  $sp^2$ -hybridized carbon frameworks,<sup>23–25</sup> and this results in great improvement of the reactivity and electrocatalytic performance of graphene. Recent reports demonstrated that nitrogen-doped graphene (NG) shows excellent electrocatalytic activity toward the oxygen reduction reaction (ORR), which reveals the possibility to replace expensive platinum-based catalysts with nitrogen-doped carbon materials and encourages us to look for highly efficient metal-free catalysts toward ORR in fuel cells.<sup>26–28</sup> Up to now, methods for NG synthesis mainly include chemical vapor deposition (CVD),<sup>21</sup> arc discharge of a graphite

\* Address correspondence to  
xhxia@nju.edu.cn,  
fbwang@nju.edu.cn.

Received for review October 21, 2010  
and accepted May 16, 2011.

Published online May 16, 2011  
10.1021/nn103584t

© 2011 American Chemical Society



**Scheme 1.** Illustration of the nitrogen doping process of melamine into GO layers. (1) Melamine adsorbed on the surfaces of GO when temperature is  $<300\text{ }^{\circ}\text{C}$ . (2) Melamine condensed and formed carbon nitride when temperature is  $<600\text{ }^{\circ}\text{C}$ . (3) Carbon nitride decomposed and doped into graphene layers when temperature is  $>600\text{ }^{\circ}\text{C}$ .

electrode in the presence of pyridine vapor,<sup>29</sup> thermal annealing GO with NH<sub>3</sub>,<sup>22,30</sup> and graphene treated with nitrogen plasma.<sup>26,27</sup> Of them, CVD is the common approach for the synthesis of NG, which employs organic molecules (e.g., CH<sub>4</sub>) as carbon source and NH<sub>3</sub> or pyridine as nitrogen source to synthesize NG via rearranging the carbon and nitrogen atoms on metal catalysts at high temperatures similar to the conditions in the synthesis of nitrogen-doped carbon nanotubes (N-CNTs).<sup>31–34</sup> In this case, metal catalysts, such as nickel and copper, are necessary to form graphene frameworks, and thus metal catalysts may remain in the resultant NG product inserting into the graphene layers. The metal impurities may interfere in explaining observed electrocatalytic properties of NG toward ORR. In addition, the nitrogen precursors of NH<sub>3</sub> and pyridine used in the CVD process are toxic, and careful treatments are essential. The toxicity of the nitrogen precursors and possible contamination of the products may limit the practical application of these gas-phase synthesis methods. In the case of the preparation of nitrogen-doped graphene using arc discharge or N<sub>2</sub> plasma, special instruments or rigorous conditions are certainly required. In order to simplify the synthetic instruments and exclude the influence of metal catalysts completely and consequently investigate the intrinsic catalytic activity of NG, developing metal-free approaches to the synthesis of NG is imperative under the situation.

In this work, we report a facile and catalyst-free approach for the synthesis of NG by thermal annealing graphite oxide (GO) using low-cost industrial material melamine as nitrogen source. X-ray photoelectron spectroscopy (XPS) was employed to evaluate the nitrogen doping degree and nitrogen bonding configurations in graphene nanosheets under different annealing conditions. It is found that nitrogen content in graphene layers up to 10.1% (atom %) can be achieved. Electrochemical results show that the resultant non-metal NGs catalyze a four-electron oxygen reduction reaction (ORR) process in alkaline electrolytes.

## RESULTS AND DISCUSSION

The preparation of NGs starts from graphite oxide (GO) through thermal annealing in the presence of melamine at 700–1000 °C in a tubular furnace. In a typical procedure, GO, synthesized by the modified Hummers' method,<sup>35,36</sup> and melamine were mixed

together with a mass ratio of 1:5 by grinding, forming a uniform gray mixture. This mixture in a crucible with a lid was then placed into a corundum tube with a flow of argon atmosphere and heated to 800 °C at a rate of 5 °C/min. After the temperature was maintained for 1 h, the furnace was cooled to room temperature slowly. The final product was collected from the crucible directly. The possible doping process is illustrated in Scheme 1. Melamine molecules first adsorbed onto GO surfaces were condensed to carbon nitride with increasing temperature in a tubular furnace.<sup>37</sup> At the same time, oxygen groups linked to graphene nanosheets in GO were removed at high temperature. We suggest it is this removal process of oxygen species that provides active sites for nitrogen doping into graphene frameworks. Nitrogen atoms or other nitrogen species formed by decomposition of carbon nitride can attack these active sites and form NGs. To a certain extent, NGs with different nitrogen atomic percent can be achieved by controlling the mass ratio of GO and melamine, the annealing temperature, and time as indicated in the XPS section. For comparison, pristine graphene was also prepared using the similar route but without adding melamine into the GO sample.

Atomic force microscopy (AFM) can directly characterize the morphologies and layers of NGs. The AFM samples were prepared by dropping NG dispersed in DMF onto clean silicon (Si) surfaces and dried at room temperature. Figure 1a shows the typical AFM image of the exfoliated NG. Flattened NG nanosheets with an average thickness of about 1.0 nm appeared, corresponding to less than three single graphene layers by considering the theoretical thickness of a single-layer graphene (~0.34 nm). Morphologies of the obtained NG were also characterized by transmission electron microscopy (TEM). As shown in the low-magnification TEM image (Figure 1b), the NG nanosheets are randomly compact and stacked together, showing uniform laminar morphology like crumpled silk veil waves similar to that of the pristine graphene (see Supporting Information, Figure S1). This morphology was attributed to defective structures formed upon exfoliation or the presence of doped nitrogen atoms.<sup>38</sup> High-resolution transmission electron micrograph (HRTEM) and selected area electron diffraction (SAED) reveal that the NG is well-crystallized, and the sharp edges made of a perfect graphitic layer with a (002) crystal plane corresponding to a *d* spacing of ~0.35 nm appear clearly

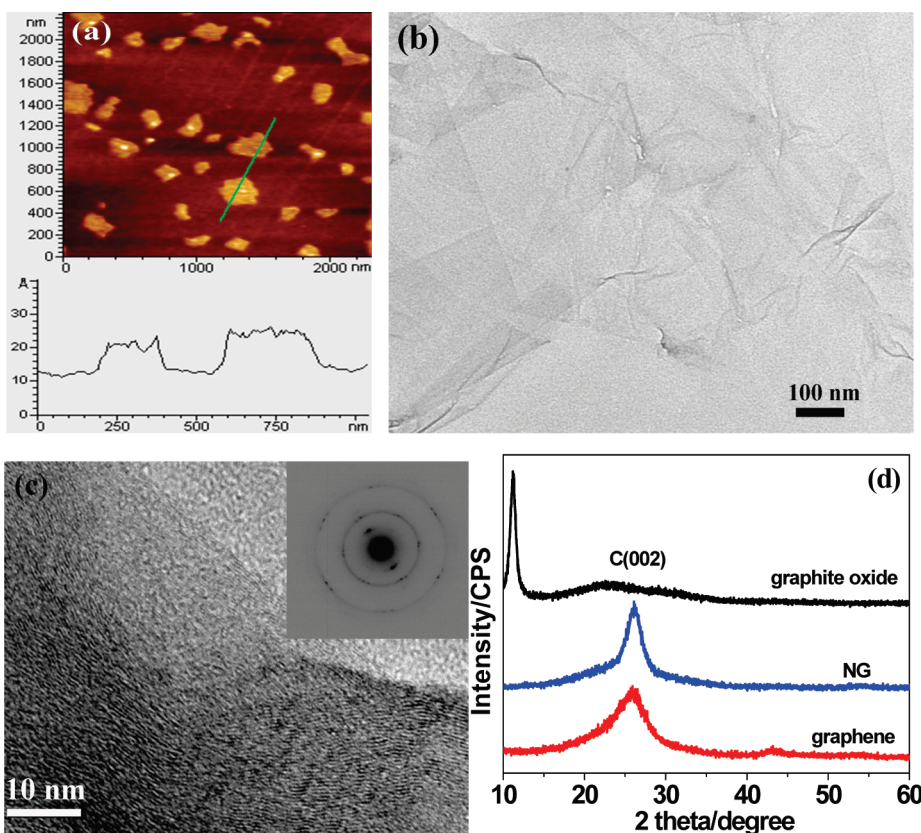


**Figure 1.** (a) Typical AFM image of NG, (b) low-resolution TEM image, and (c) high-resolution TEM image and selected area electron diffraction (SAED) pattern (inset) of NG. (d) Typical PXRD patterns of NG (blue), graphite oxide (black), and pristine graphene (red).

(Figure 1c), which is closer to that of single-crystal graphite (0.335 nm). In SAED, the well-defined diffraction spots and rings are fully indexed to the typical hexagonal lattice of carbon in NG, confirming the crystalline nature of NG prepared *via* thermal annealing GO with melamine.<sup>39</sup> On the other hand, the PXRD pattern (Figure 1d) of NG shows a broad peak around 26.0° with an interlayer space of ~0.34 nm (for pristine graphene, the strong diffraction peak locates at 25.8°), which is similar to that of the HRTEM result. GO's diffraction peak indexed to (002) shifts negatively to ~11.2°, corresponding to a layered structure with a basal spacing of 0.79 nm.<sup>40</sup> These results demonstrate that thermal annealing of GO will partially restore the graphitic crystal structure due to the reduction effect of high temperature and nitrogen doping. The Brunauer–Emmett–Teller (BET) specific surface areas of the pristine graphene and nitrogen-doped graphene (NG5 prepared by annealing GO and melamine with a mass ratio of 1:5 at 800 °C for 0.5 h) are measured from the nitrogen adsorption–desorption isotherms at 77 K. It is found that the specific surface area of pristine graphene is 281 m<sup>2</sup>/g, which is significantly lower than the theoretical surface area of 2630 m<sup>2</sup>/g for individual isolated graphene sheets.<sup>9</sup> However, the specific surface area of sample NG5 is only 6 m<sup>2</sup>/g, which is smaller than that of the pristine graphene. From the specific surface

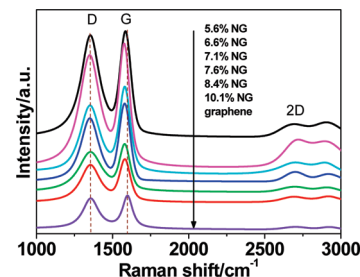


**Figure 2.** Raman spectra of pristine graphene (violet) and NGs with different nitrogen atomic percentage: 5.6% (black), 6.6% (magenta), 7.1% (cyan), 7.6% (blue), 8.4% (green), and 10.1% (red), respectively.

area of NG5 and the pristine graphene, the graphene and nitrogen-doped graphene synthesized by the thermal annealing method contain more than one layer of graphene sheets, which is consistent with the observations from AFM, TEM, and Raman characterizations.

Raman spectroscopy is the most direct and nondestructive technique to characterize the structure and quality of carbon materials,<sup>41</sup> particularly to determine the defects, the ordered and disordered structures, and the layers of graphene. Therefore, Raman spectra of the as-made NGs were collected by micro-Raman spectroscopy at an excitation wavelength of 514 nm under ambient conditions by dropping the DMF dispersions on Si substrates. For comparison, the spectra of GO and

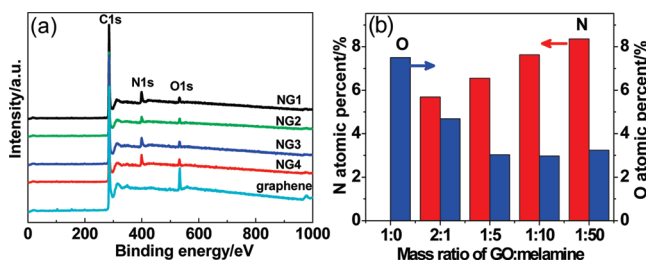


**Figure 3.** (a) XPS spectra of the pristine graphene, NGs prepared with GO/melamine mass ratio of 1:5 at 700 °C (NG1) and at 800 °C (NG2), and NGs prepared with GO/melamine mass ratio of 1:10 (NG3) and 1:50 (NG4) at 800 °C. (b) Atomic percentage of nitrogen (red) and oxygen (blue) in NGs obtained by annealing the precursors with different mass ratio of GO/melamine at 800 °C.

pristine graphene obtained from thermally annealing GO under the same conditions were also collected. The Raman spectra of NGs exhibit two remarkable peaks at around 1350 and 1580 cm<sup>-1</sup> (Figure 2) corresponding to the well-defined D band and G band, respectively. The G band of the pristine graphene prepared under similar conditions is up-shifted to 1595 cm<sup>-1</sup> as compared with NGs (~1580 cm<sup>-1</sup>). This phenomenon arising from nitrogen doping is similar to the results of nitrogen-doped CNTs.<sup>24</sup> As is known, the G band related to the E<sub>2g</sub> vibration mode of sp<sup>2</sup> carbon domains can be used to explain the degree of graphitization, while the D band is associated with structural defects and partially disordered structures of the sp<sup>2</sup> domains.<sup>42</sup> It clearly shows that the intensity of the D band in pure graphene and NGs is lower than that of GO ( $I_D/I_G = 1.02$ ; see Supporting Information, Figure S2), and the  $I_D/I_G$  values of NGs decrease to 0.86–0.98 due to different synthetic conditions. This indicates that partial sp<sup>2</sup> domains were restored at different levels, and the graphitic degree of NG samples was also improved accordingly due to the reduction effect and “self-repairing” of the graphene layer at high temperature. In addition, the  $I_D/I_G$  values of NGs were similar to that of the pristine graphene ( $I_D/I_G = 0.88$ ) synthesized at similar conditions, which indicates that graphitization degree of the resultant NGs is analogous to the pristine graphene. The 2D peak is the most prominent feature of graphene in the Raman spectrum, and its position and shape can be used to clearly distinguish between single-layer, bilayer, and few-layer graphenes. For the as-made NGs, the 2D peaks appear at around 2700 cm<sup>-1</sup>. Compared with the spectrum of single-layer graphene,<sup>43</sup> the present NGs exhibit a broader and up-shifted peak in the Raman spectra, demonstrating that the present thermal annealing process results in few-layer NGs. This result is consistent with the AFM and TEM characterizations. However, single-layer NGs could be obtained when the single-layer GO precursor on a silicon substrate surface is prepared. Thermal annealing of the single-layer GO nanosheets covered with melamine would result in a single layer of nitrogen-doped graphene nanosheets.

X-ray photoelectron spectroscopy (XPS) characterizations were further performed to analyze the elemental composition and nitrogen bonding configurations in

NGs. As is shown in Figure 3a, the XPS spectrum of the pristine graphene shows only the presence of carbon and oxygen atoms. XPS spectra for NG samples clearly show the incorporation of nitrogen atoms within the graphene sheets, and the calculated N/C atomic ratio is in the range of ~0.06–0.12 by controlling the annealing temperature, the annealing time, and the amount of melamine. Combined with the above Raman and microscopic results, NGs can be successfully synthesized by thermal annealing GO in the presence of melamine. Moreover, the nitrogen content in NGs can be tailored by controlling the synthetic conditions. Under the conditions of 700 °C with a 0.2 mass ratio of GO to melamine, the highest doping level of 10.1% (atom %) can be achieved. Once the annealing temperature was increased to 800 °C, the nitrogen doping level decreased to 6.6% immediately. While the annealing temperature is kept constant, the doping level will increase with the increase of melamine mass (Figure 3b). It is interesting to find that the percentage of oxygen is lower in the NGs than in the pristine graphene when the samples are prepared at the same annealing temperature and time. As shown in Figure 3b, the atomic percentages of oxygen in graphene and NG3 prepared at 800 °C are 7.5 and 3.0%, respectively, indicating that nitrogen doping increases the reduction efficiency of GO. In addition, the oxygen level becomes lower with the decrease of GO/melamine mass ratio. At GO/melamine mass ratio of 1:10, the lowest atomic percentage (3.0%) of oxygen in the resultant sample is obtained. These phenomena are in good agreement with Dai's previous report<sup>30</sup> and could be due to the competitive doping between oxygen and melamine. To further confirm the nitrogen doping of graphene, electron energy loss spectroscopy (EELS) measurements were also carried out. Typical EELS spectrum (see Supporting Information, Figure S3) shows two visible edges located at ~277 and ~396 eV corresponding to the characteristic K-shell ionization edges of C and N, respectively. As a result, the two bands corresponding to C and N can be well-confirmed, and nitrogen doping of graphene is really achieved using our approach. This result is consistent with the one from XPS measurements. Band for the K-shell ionization edges of O is invisible. The characteristic K-edge of N appeared at 398 eV with  $\pi^*$  and  $\sigma^*$  peaks

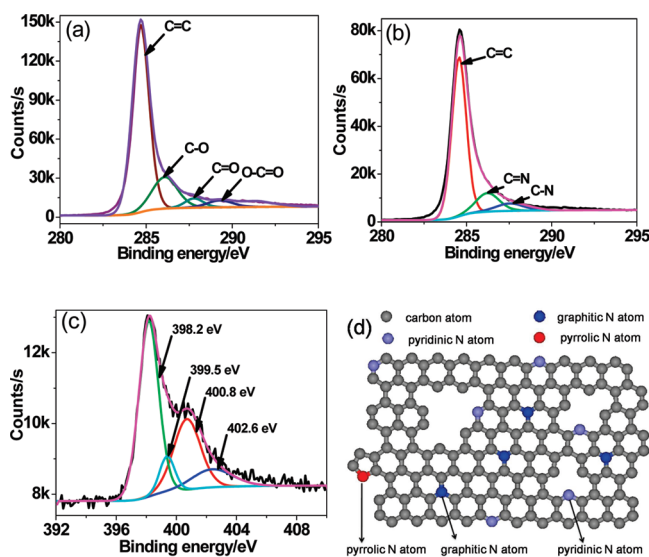


**Figure 4.** (a) High-resolution C1s spectra of the pristine graphene prepared at 800 °C by thermal annealing. C1s (b) and N1s (c) spectra of NG prepared at 800 °C by thermal annealing with GO/melamine mass ratio of 1:5 for 30 min (nitrogen atomic percentage is 7.1%, denoted as NG5). (d) Schematic structure of NG.

**TABLE 1. Carbon Atomic Percent of NGs Prepared by Annealing GO and Melamine for 1 h under Different Mass Ratio and Temperature<sup>a</sup>**

	NG1	NG2	NG3	NG4
C% (atom %)	86.8	90.4	89.4	88.4
N% (atom %)	10.1	6.6	7.6	8.4

<sup>a</sup> GO/melamine = 1:5 at 700 °C (NG1), GO/melamine = 1:5 at 800 °C (NG2), GO/melamine = 1:10 at 800 °C (NG3), and GO/melamine = 1:50 at 800 °C (NG4).

indicating that  $sp^2$ -hybridized N atoms were indeed incorporated into the graphene layers.<sup>44–46</sup>

The high-resolution C1s XPS spectra of the as-made samples show one main peak at 284.4–284.8 eV, corresponding to  $sp^2$ -hybridized graphitic carbon atoms and small signals at higher binding energy (BE) indicating some C–N and/or C–O species remaining in the samples after thermal annealing.<sup>40</sup> In the C1s spectra of the pristine graphene, the sharp peak at 284.5 eV corresponding to  $sp^2$  carbon atoms indicates most of carbon atoms being in the form of conjugated honeycomb lattice, and the peaks at 286.2, 287.8, and 289.2 eV, which are attributed to different C–O bonding configurations, decrease considerably after thermal annealing of GO (Figure 4a and Figure S4a in Supporting Information). This reveals that most of the oxygen groups have been removed, and the graphitic carbon network was partially restored. Due to the disordering of the graphite-like structure after introduction of nitrogen atoms into graphene layers, the sharp peak in the C1s spectrum of NGs, which is still assigned to the graphitic  $sp^2$  carbon atoms, shifts to higher binding energies of 284.6–284.8 eV.<sup>47</sup> On the other hand, from the XPS results, the carbon content (atom %) in NGs decreases slightly with the increase of nitrogen atomic percentage (Table 1). However, the peaks at ~284.7 eV are still the

**TABLE 2. Percentage of Carbon atoms and Full Width at Half-Maximum Values of C1s Peaks in Graphene, NGs with 7.1% (NG5), and 10.1% (NG1) Nitrogen**

	carbon % (atom %)	fwhm (eV)
NG1	86.8	1.23
NG5	89.8	1.21
graphene	92.5	1.14

largest ones in the C1s spectra (see Supporting Information, Figure S4b), indicating the partial reconstruction of graphene structures during the nitrogen doping process. The small new peaks at 285.8 and 287.5 eV obtained by peak fitting suggest the bonding formation of doped nitrogen atoms to be  $sp^2$ -C and  $sp^3$ -C atoms, respectively (Figure 4b). Compared with the pristine graphene, the high-resolution C1s peak of NGs shifts to high binding energy and its full width of half-maximum (fwhm) at 284.6 eV increases with the increase of nitrogen content (Table 2). All of these results indicate the formation of C–N bonds in the annealing process.

Similarly, the bonding configurations of nitrogen atoms in NGs were characterized by high-resolution N1s spectra. For example, the N1s spectra of NG5 can be fitted into four peaks at 398.2, 399.5, 401.1, and 402.6 eV (Figure 4c). The peaks with lower binding energy located at about 398.2 and 399.5 eV, respectively, correspond to pyridine-like and pyrrole-like nitrogen, as illustrated in Figure 4d, which can contribute to the  $\pi$ -conjugated system with a pair of p-electrons in the graphene layers. When carbon atoms within the graphene layers are substituted by nitrogen atoms in the form of “graphitic” nitrogen, the corresponding peak in the high-resolution N1s spectra is located at 400.8–401.3 eV. It is also found that increasing the annealing temperature results in more

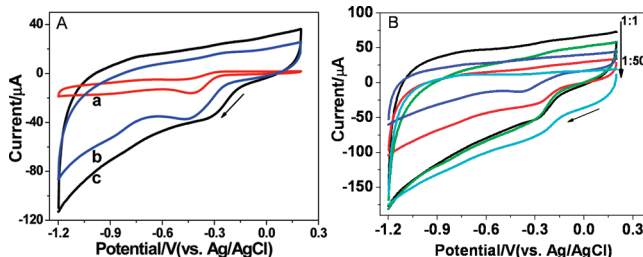


**Figure 5.** (A) Typical cyclic voltammograms (CVs) for ORR obtained at a bare GCE (a), graphene/GCE (b), and NG5/GCE (N% = 7.1%) (c) in  $O_2$  saturated 0.1 M KOH aqueous solution. (B) CVs for ORR at NGs, synthesized with different mass ratio of GO and melamine (1:1, 1:2, 1:5, 1:10, 1:50) at 800  $^{\circ}$ C, modified GCE in  $O_2$  saturated 0.1 M KOH aqueous solution. Scan rate: 100 mV/s.

graphitic N incorporated into the graphene networks. The high energy peak at 402.3–402.9 eV is commonly attributed to oxidized nitrogen.<sup>48</sup> As shown by the N1s spectra, pyridine-like nitrogen is the main component in our prepared NGs (Figure 4c and Figure S5 in Supporting Information). Our results demonstrate that it is not the quantity of nitrogen precursor melamine but the annealing temperature that can be the key factor to modulate the chemical state of nitrogen in doped graphene (see Supporting Information, Table S1).

The oxygen reduction reaction (ORR) is of great importance in fuel cells and other electrochemical devices.<sup>49</sup> Recently, great efforts have been focused on developing effective and low-cost ORR electrocatalysts, including nonmetal carbon materials.<sup>28,50,51</sup> Consequently, NG as a special kind of carbon material was also used in electrocatalytic application of ORR. Cyclic voltammetry and rotating ring-disk electrode (RRDE) technique were taken to explain the electrocatalytic activity of NGs toward the ORR. Figure 5A shows the cyclic voltammograms (CVs) for the electrochemical reduction of  $O_2$  at a bare glassy carbon electrode (GCE), graphene/GCE, and NG5/GCE in  $O_2$  saturated 0.1 M KOH aqueous solution. For the bare GCE and pure graphene/GCE, the electrochemical reduction occurs in two processes with onset potentials at around −0.3, −0.7 V and −0.2, −0.6 V, respectively. Clearly, the graphene/GCE exhibits more positive onset potential and much larger reduction current for ORR (Figure 5A, curve b), indicating a much faster electron transfer kinetics for ORR on graphene than on a bare GCE. Interestingly, the onset potential of ORR on the NG5/GCE occurs at −0.1 V, which is about 0.1 V more positive than on graphene/GCE. In addition, compared to the pristine graphene, the reduction current for ORR catalyzed by NG5 is much larger. Both the positive shift of onset potential and the enhanced reduction current for ORR on NG5/GCE demonstrate that NG5 possesses much higher electrocatalytic activity toward ORR than graphene, which could be due to a faster reaction kinetics with a higher transferred electron number per oxygen molecule at the NG5 modified electrode surface. To further evaluate the transferred electron number (*n*) per oxygen molecule at the NG5/GCE, RRDE

testing was performed using a NG5/GC disk Pt ring electrode. The results are shown in Supporting Information (Figure S6a). Although the electrocatalytic activity of NG5 toward ORR is lower than that in the bulk platinum disk, it is much better than graphene and glassy carbon. The calculated *n* value for the pure graphene is about 2.2–2.4 at potentials ranging from −0.3 to −0.8 V (see Supporting Information, Figure S6b), which explains that the ORR process catalyzed by the pure graphene/GCE is a two-step two-electron pathway with the formation of intermediate  $HO_2^-$  ions. The first process could be attributed to the reduction of  $O_2$  to peroxide, which is electrochemically mediated by the oxygen-containing surface groups, while the second is a direct  $2e^-$  reduction process at the electrode.<sup>52</sup> However, the *n* value for NG5 is about 3.4–3.6 at potentials ranging from −0.3 to −0.8 V, which reveals that the electrocatalytic process of NG5/GCE is a one-step four-electron pathway for ORR with much higher peak current, which is similar to the recent report.<sup>46</sup> Electrocatalytic selectivity and stability were also measured by exposing NG5/GCE to the fuel molecule methanol (see Supporting Information, Figure S7). It shows that the addition of 1.0 M methanol does not affect the electrocatalytic activities of NG toward ORR, which indicates that NG5 possesses excellent selectivity and stability toward ORR in 0.1 M KOH aqueous solution. These results suggest that NGs are a promising nonmetal catalyst for the ORR in alkaline solutions. The excellent electrocatalytic activity of NGs could be attributed to the incorporation of nitrogen atoms into the graphene layers, which favors the reactivity of the neighborly linked carbon atoms *via* alteration of the electronic structure as in the case of nitrogen-doped CNTs.<sup>53</sup>

To investigate the effect of nitrogen content in doped graphene nanosheets, the electrocatalytic activity of NGs with different nitrogen content toward the ORR process in oxygen saturated 0.1 M KOH aqueous solution was studied. The CVs show similar electrochemical behavior for the ORR at all the NGs modified GCE. However, the reduction current increases with the increase of nitrogen content in NGs (Figure 5B). The onset potential of ORR is around −0.1 V and almost invariable with the increase of nitrogen content. This

demonstrates that the nitrogen content in NGs does not significantly affect the electrocatalytic activity of NGs toward ORR. It may imply that the pyridine-like nitrogen component in NGs determines the electrocatalytic activity of NGs toward ORR because nitrogen bonding configurations in NGs in the present work are composed mainly of pyridinic nitrogen. As a result, it is not the nitrogen content but the nitrogen bonding configurations in NGs that could be the key factor for electrocatalytic performance toward ORR.

## CONCLUSIONS

In summary, we report a facile, catalyst-free thermal annealing method to prepare NGs in larger scale using low-cost industrial material melamine as the nitrogen source. In this method, the atomic percent of nitrogen in graphene layers can be adjusted up to 10.1% as estimated from the XPS analysis. High-resolution N1s spectra reveal that all of the nitrogen atoms are mainly in the form of pyridine-like bonding configuration in

NGs synthesized by thermal annealing GO with melamine. It is also found that the content of graphitic nitrogen will increase with higher annealing temperature. The present synthesis method can also be extended to prepare other element (such as B, Si, P, and S)-doped graphene nanosheets if appropriate precursors are used. Electrochemical characterizations demonstrate that the NGs exhibit excellent electrocatalytic activities toward ORR in alkaline electrolytes, similar to what was observed in nitrogen-doped vertically aligned carbon nanotubes. Since the electrocatalytic activity of the NGs toward ORR is not considerably affected by the alteration of nitrogen content in NGs, it may imply that the pyridine-like nitrogen component in NGs determines the electrocatalytic activity of NGs toward ORR. Thus, searching for an effective doping approach and illuminating the electrocatalytic mechanisms of NGs toward ORR should be of great importance for the development of nonmetal ORR catalysts, even practical applications in fuel cells and biosensors.

## METHODS

**Materials.** Graphite powder (99.9995% purity, -100 mesh, briquetting grade, mesh) was purchased from Alfa Aesar. Melamine was bought from Sinopharm Chemical Reagent CO. Ltd. (China) and used after recrystallization from water. Other chemicals such as H<sub>2</sub>SO<sub>4</sub>, KOH, and *N,N*-dimethylformamide (DMF), bought from Nanjing Chemical Reagent CO. Ltd., were all of analytical grade and used as received. All solutions used in the electrochemical experiments were freshly prepared with Millipore water having a resistivity of 18.2 MΩ (Purelab Classic Corp., USA).

**Apparatus.** The morphology of graphene and NG samples was characterized by transmission electron microscopy (TEM) and HRTEM using a Hitachi-2100 TEM facility with a 200 kV accelerating voltage. The TEM samples were prepared by drying a droplet of the graphene or NG suspensions on a Cu grid with carbon film. Atomic force microscopy (AFM) images were obtained on an Agilent 5500 AFM/SPM system with Picoscan v5.3.3 software. Imaging was performed in tapping mode under ambient conditions. An X-ray powder diffractometer (XRD, Shimadzu, X-6000, Cu Kα radiation) was used to determine the phase purity and crystallization degree. Room temperature Raman spectra were recorded using a Renishaw InVia micro-Raman system with an excitation wavelength of 514 nm. X-ray photoelectron spectroscopy (XPS, Kα) analyses were carried out on a Thermo Fisher X-ray photoelectron spectrometer system equipped with Al radiation as a probe, with a chamber pressure of  $5 \times 10^{-9}$  Torr. The source power was set at 72 W, and pass energies of 200 eV for survey scans and 50 eV for high-resolution scans were used. The analysis spot size was 400 μm in diameter. All electrochemical measurements were performed on a CHI 900 electrochemical workstation (CH Instruments, USA). Cyclic voltammograms were collected in a three-electrode system (GCE or modified GCE as the working electrode, a Pt wire as counter electrode, and an Ag/AgCl as the reference) at room temperature. For RRDE measurements, a HP-1A RRDE system from Jiangfen Electroanalytical Instrument Co. Ltd., China, was used as the working electrode. This RRDE consists of a GC disk (4 mm in diameter) and Pt ring electrodes (1 mm in width). For RRDE measurements, the Pt ring electrode was modified with 5 μL of 1 mg/mL graphene or NG suspensions. The collection efficiency of the RRDE was determined to be 0.47 using Fe(CN)<sub>6</sub><sup>4-/3-</sup> as electrochemical probe. Linear sweep voltammetry was performed at the GC disk electrode, while the Pt ring electrode was polarized at 0.5 V for oxidizing

intermediates generated from the disk electrode. In all of the electrochemical measurements, 0.1 M KOH aqueous solution saturated with oxygen was used as the electrolyte.

**Synthesis of Nitrogen-Doped Graphene Nanosheets.** Annealing of GO was carried out in a homemade tube furnace. We used high-purity argon as protective ambient to anneal GO or a mixture of GO and melamine. Detailed procedure is as follows: GO powder and melamine were ground together in a mortar using pestle for about 5 min, and the mixture was then placed in the center of a corundum tube with a flow of argon. Before the furnace was heated to 300 °C, Ar gas was flowed for about 20 min. When the center of the furnace reached the designed reaction temperature (e.g., 800 °C), the mixture was annealed for 1 h at this temperature. After that, the sample was cooled to room temperature under Ar ambient. Finally, the products were taken out of the corundum tube. The pristine graphene was synthesized from GO using a similar procedure but without melamine.

**Preparation of Graphene, Nitrogen-Doped Graphene Modified Electrode.** Prior to use, glassy carbon electrode (GCE, φ = 3 mm) was polished with 0.05 μm gamma alumina powders, then rinsed thoroughly with ethanol and water in an ultrasonic bath to remove any alumina residues, and finally dried with blowing N<sub>2</sub> gas. Ten microliters of sonicated pure graphene or NG DMF suspension was dropped on the pretreated bare GCE using a micropipet tip and dried in air.

**Acknowledgment.** This work was supported by grants from the National 973 Basic Research Program (2007CB714501), the National Natural Science Foundation of China (NSFC, Nos. 20828006 and 21035002), the National Science Fund for Creative Research Groups (20821063), and the Natural Science Foundation of Jiangsu province (BK2010009).

**Supporting Information Available:** TEM image of pristine graphene, Raman spectrum of GO, XPS results, and RRDE voltammograms for ORR at different electrodes. This material is available free of charge via the Internet at <http://pubs.acs.org>.

## REFERENCES AND NOTES

- Allen, M. J.; Tung, V. C.; Kaner, R. B. Honeycomb Carbon: A Review of Graphene. *Chem. Rev.* **2010**, *110*, 132–145.
- Rao, C. N. R.; Sood, A. K.; Subrahmanyam, K. S.; Govindaraj, A. Graphene: The New Two Dimensional Nanomaterial. *Angew. Chem., Int. Ed.* **2009**, *48*, 7752–7777.

3. Geim, A. K.; Novoselov, K. S. The Rise of Graphene. *Nat. Mater.* **2007**, *6*, 183–191.
4. Lee, C. G.; Wei, X. D.; Kysar, J. W.; Hone, J. Measurement of the Elastic Properties and Intrinsic Strength of Monolayer Graphene. *Science* **2008**, *321*, 385–388.
5. Novoselov, K. S.; Geim, A. K.; Morozov, S. V.; Jiang, D.; Katsnelson, M. I.; Grigorieva, I. V.; Dubonos, S. V.; Firsov, A. A. Two-Dimensional Gas of Massless Dirac Fermions in Graphene. *Nature* **2005**, *438*, 197–200.
6. Pang, S. P.; Tsao, H. N.; Feng, X. L.; Müllen, K. Patterned Graphene Electrodes from Solution-Processed Graphite Oxide Films for Organic Field-Effect Transistors. *Adv. Mater.* **2009**, *21*, 3488–3491.
7. Wang, S.; Ang, P. K.; Wang, Z. Q.; Tang, A. L. L.; Thong, J. T. L.; Loh, K. P. High Mobility, Printable, and Solution-Processed Graphene Electronics. *Nano Lett.* **2010**, *10*, 92–98.
8. Wang, X.; Zhi, L. J.; Müllen, K. Transparent, Conductive Graphene Electrodes for Dye-Sensitized Solar Cells. *Nano Lett.* **2008**, *8*, 323–327.
9. Stoller, M. D.; Park, S. J.; Zhu, Y. W.; An, J. H.; Ruoff, R. S. Graphene-Based Ultracapacitors. *Nano Lett.* **2008**, *8*, 3498–3502.
10. Elias, D. C.; Nair, R. R.; Mohiuddin, T. M. G.; Morozov, S. V.; Blake, P.; Halsall, M. P.; Ferrari, A. C.; Boukhvalov, D. W.; Katsnelson, M. I.; Geim, A. K.; et al. Control of Graphene's Properties by Reversible Hydrogenation: Evidence for Graphane. *Science* **2009**, *323*, 610–613.
11. Stankovich, S.; Dikin, D. A.; Domke, G. H. B.; Kohlhaas, K. M.; Zimney, E. J.; Stach, E. A.; Piner, R. D.; Nguyen, S. T.; Ruoff, R. S. Graphene-Based Composite Materials. *Nature* **2006**, *442*, 282–286.
12. Ramanathan, T.; Abdala, A. A.; Stankovich, S.; Dikin, D. A.; Herrera-Alonso, M.; Piner, R. D.; Adamson, D. H.; Schniepp, H. C.; Chen, X.; Ruoff, R. S.; et al. Functionalized Graphene Sheets for Polymer Nanocomposites. *Nat. Nanotechnol.* **2008**, *3*, 327–331.
13. Robinson, J. T.; Perkins, F. K.; Snow, E. S.; Wei, Z. Q.; Sheehan, P. E. Reduced Graphene Oxide Molecular Sensors. *Nano Lett.* **2008**, *8*, 3137–3140.
14. Guo, S. J.; Wen, D.; Zhai, Y. M.; Dong, S. J.; Wang, E. K. Platinum Nanoparticle Ensemble-on-Graphene Hybrid Nanosheet: One-Pot, Rapid Synthesis, and Used as New Electrode Material for Electrochemical Sensing. *ACS Nano* **2010**, *4*, 3959–3968.
15. Lu, C. H.; Yang, H. H.; Zhu, C. L.; Chen, X.; Chen, G. N. A Graphene Platform for Sensing Biomolecules. *Angew. Chem., Int. Ed.* **2009**, *48*, 4785–4787.
16. Kim, K. S.; Zhao, Y.; Jang, H.; Lee, S. Y.; Kim, J. M.; Kim, K. S.; Ahn, J. H.; Kim, P.; Choi, J. Y.; Hong, B. H. Large-Scale Pattern Growth of Graphene Films for Stretchable Transparent Electrodes. *Nature* **2009**, *457*, 706–710.
17. Reina, A.; Jia, X. T.; Ho, J.; Nezich, D.; Son, H. B.; Bulovic, V.; Dresselhaus, M. S.; Kong, J. Large Area, Few-Layer Graphene Films on Arbitrary Substrates by Chemical Vapor Deposition. *Nano Lett.* **2009**, *9*, 30–35.
18. Li, X. L.; Zhang, G. Y.; Bai, X. D.; Sun, X. M.; Wang, X. R.; Wang, E. G.; Dai, H. J. Highly Conducting Graphene Sheets and Langmuir–Blodgett Films. *Nat. Nanotechnol.* **2008**, *3*, 538–542.
19. Park, S.; An, J.; Jung, I.; Piner, R. D.; An, S. J.; Li, X.; Velamakanni, A.; Ruoff, R. S. Colloidal Suspensions of Highly Reduced Graphene Oxide in a Wide Variety of Organic Solvents. *Nano Lett.* **2009**, *9*, 1593–1597.
20. Li, X. L.; Wang, X. R.; Zhang, L.; Lee, S.; Dai, H. J. Chemically Derived, Ultrasmooth Graphene Nanoribbon Semiconductors. *Science* **2008**, *319*, 1229–1232.
21. Wei, D. C.; Liu, Y. Q.; Wang, Y.; Zhang, H. L.; Huang, L. P.; Yu, G. Synthesis of N-Doped Graphene by Chemical Vapor Deposition and Its Electrical Properties. *Nano Lett.* **2009**, *9*, 1752–1758.
22. Wang, X. R.; Li, X. L.; Zhang, L.; Yoon, Y. K.; Weber, P. K.; Wang, H. L.; Guo, J.; Dai, H. J. N-Doping of Graphene through Electrothermal Reactions with Ammonia. *Science* **2009**, *324*, 768–771.
23. Gong, K. P.; Du, F.; Xia, Z. H.; Durstock, M.; Dai, L. M. Nitrogen-Doped Carbon Nanotube Arrays with High Electrocatalytic Activity for Oxygen Reduction. *Science* **2009**, *323*, 760–764.
24. Panchakarla, L. S.; Govindaraj, A.; Rao, C. N. R. Nitrogen- and Boron-Doped Double-Walled Carbon Nanotubes. *ACS Nano* **2007**, *1*, 494–500.
25. Zhang, J.; Liu, X.; Blume, R.; Zhang, A.; Schlögl, R.; Su, D. Surface-Modified Carbon Nanotubes Catalyze Oxidative Dehydrogenation of n-Butane. *Science* **2008**, *322*, 73–77.
26. Wang, Y.; Shao, Y. Y.; Matson, D. W.; Li, J. H.; Lin, Y. H. Nitrogen-Doped Graphene and Its Application in Electrochemical Biosensing. *ACS Nano* **2010**, *4*, 1790–1798.
27. Shao, Y. Y.; Zhang, S.; Engelhard, M. H.; Li, G. S.; Shao, G. C.; Wang, Y.; Liu, J.; Aksay, I. A.; Lin, Y. H. Nitrogen-Doped Graphene and Its Electrochemical Applications. *J. Mater. Chem.* **2010**, *20*, 7491–7496.
28. Qu, L. T.; Liu, Y.; Baek, J. B.; Dai, L. M. Nitrogen-Doped Graphene as Efficient Metal-Free Electrocatalyst for Oxygen Reduction in Fuel Cells. *ACS Nano* **2010**, *4*, 1321–1326.
29. Panchakarla, L. S.; Subrahmanyam, K. S.; Saha, S. K.; Govindaraj, A.; Krishnamurthy, H. R.; Waghmare, U. V.; Rao, C. N. R. Synthesis, Structure and Properties of Boron and Nitrogen Doped Graphene. *Adv. Mater.* **2009**, *21*, 4726–4730.
30. Li, X. L.; Wang, H. L.; Robinson, J. T.; Sanchez, H.; Diankov, G.; Dai, H. J. Simultaneous Nitrogen Doping and Reduction of Graphene Oxide. *J. Am. Chem. Soc.* **2009**, *131*, 15939–15944.
31. Pumera, M. Carbon Nanotubes Contain Residual Metal Catalyst Nanoparticles Even after Washing with Nitric Acid at Elevated Temperature Because These Metal Nanoparticles Are Sheathed by Several Graphene Sheets. *Langmuir* **2007**, *23*, 6453–6458.
32. Hiura, H.; Ebbesen, T.; Tanigaki, K. Opening and Purification of Carbon Nanotubes in High Yields. *Adv. Mater.* **1995**, *7*, 275–276.
33. Ebbesen, T.; Ajayan, P.; Tanigaki, K. Purification of Nanotubes. *Nature* **1994**, *367*, 519–519.
34. Pumera, M.; Iwai, H. Multicomponent Metallic Impurities and Their Influence upon the Electrochemistry of Carbon Nanotubes. *J. Phys. Chem. C* **2009**, *113*, 4401–4405.
35. Hummers, W. S.; Offeman, R. E. Preparation of Graphitic Oxide. *J. Am. Chem. Soc.* **1958**, *80*, 1339–1339.
36. Guo, H. L.; Wang, X. F.; Qian, Q. Y.; Wang, F. B.; Xia, X. H. A Green Approach to the Synthesis of Graphene Nanosheets. *ACS Nano* **2009**, *3*, 2653–2659.
37. Groenewolt, M.; Antonietti, M. Synthesis of g-C3N4 Nanoparticles in Mesoporous Silica Host Matrices. *Adv. Mater.* **2005**, *17*, 1789–1792.
38. Meyer, J. C.; Geim, A. K.; Katsnelson, M. I.; Novoselov, K. S.; Booth, T. J.; Roth, S. The Structure of Suspended Graphene Sheets. *Nature* **2007**, *446*, 60–63.
39. Hernandez, Y.; Nicolosi, V.; Lotya, M.; Blighe, F. M.; Sun, Z.; De, S.; McGovern, I. T.; Holland, B.; Byrne, M.; Gun'ko, Y. K.; et al. High-Yield Production of Graphene by Liquid-Phase Exfoliation of Graphite. *Nat. Nanotechnol.* **2008**, *3*, 563–568.
40. Jeong, H. K.; Lee, Y. P.; Lahaye, R. J.; Park, M. H.; An, K. H.; Kim, I. J.; Yang, C. W.; Park, C. Y.; Ruoff, R. S.; Lee, Y. H. Evidence of Graphitic AB Stacking Order of Graphite Oxides. *J. Am. Chem. Soc.* **2008**, *130*, 1362–1366.
41. Das, A.; Pisana, S.; Chakraborty, B.; Piscanec, S.; Saha, S. K.; Waghmare, U. V.; Novoselov, K. S.; Krishnamurthy, H. R.; Geim, A. K.; Ferrari, A. C.; et al. Monitoring Dopants by Raman Scattering in an Electrochemically Top-Gated Graphene Transistor. *Nat. Nanotechnol.* **2008**, *3*, 210–215.
42. Kudin, K. N.; Ozbas, B.; Schniepp, H. C.; Prud'homme, R. K.; Aksay, I. A.; Car, R. Raman Spectra of Graphite Oxide and Functionalized Graphene Sheets. *Nano Lett.* **2008**, *8*, 36–41.
43. Lui, C. H.; Liu, L.; Mak, K. F.; Flynn, G. W.; Heinz, T. F. Ultraflat Graphene. *Nature* **2009**, *462*, 339–341.
44. Stephan, O.; Ajayan, P. M.; Colliex, C.; Redlich, Ph.; Lambert, J. M.; Bernier, P.; Lefin, P. Doping Graphitic and Carbon Nanotube Structures with Boron and Nitrogen. *Science* **1994**, *266*, 1683–1685.
45. Ci, L.; Song, L.; Jin, C.; Jariwala, D.; Wu, D.; Li, Y.; Srivastava, A.; Wang, Z. F.; Storr, K.; Balicas, L.; et al. Atomic Layers of Hybridized Boron Nitride and Graphene Domains. *Nat. Mater.* **2010**, *9*, 430–435.

46. Song, L.; Ci, L.; Lu, H.; Sorokin, P. B.; Jin, C.; Ni, J.; Kvashnin, A. G.; Kvashnin, D. G.; Lou, J.; Yakobson, B. I. Large Scale Growth and Characterization of Atomic Hexagonal Boron Nitride Layers. *Nano Lett.* **2010**, *10*, 3209–3215.
47. Ayala, P.; Grüneis, A.; Gemming, T.; Büchner, B.; Rümmeli, M. H.; Grimm, D. Influence of the Catalyst Hydrogen Pretreatment on the Growth of Vertically Aligned Nitrogen-Doped Carbon Nanotubes. *Chem. Mater.* **2007**, *19*, 6131–6137.
48. Xu, F.; Minniti, M.; Barone, P.; Sindona, A.; Bonanno, A.; Oliva, A. Nitrogen Doping of Single Walled Carbon Nanotubes by Low Energy N<sub>2</sub><sup>+</sup> Ion Implantation. *Carbon* **2008**, *46*, 1489–1496.
49. Steele, B. C. H.; Heinzel, A. Materials for Fuel-Cell Technologies. *Nature* **2001**, *414*, 345–352.
50. Liu, R. L.; Wu, D. Q.; Feng, X. L.; Müllen, K. Nitrogen-Doped Ordered Mesoporous Graphitic Arrays with High Electrocatalytic Activity for Oxygen Reduction. *Angew. Chem., Int. Ed.* **2010**, *49*, 2565–2569.
51. Tang, Y. F.; Allen, B. L.; Kauffman, D. R.; Star, A. Electrocatalytic Activity of Nitrogen-Doped Carbon Nanotube Cups. *J. Am. Chem. Soc.* **2009**, *131*, 13200–13201.
52. Zhang, M. N.; Yan, Y. M.; Gong, K. P.; Mao, L. Q.; Guo, Z. X.; Chen, Y. Electrostatic Layer-by-Layer Assembled Carbon Nanotube Multilayer Film and Its Electrocatalytic Activity for O<sub>2</sub> Reduction. *Langmuir* **2004**, *20*, 8781–8785.
53. Chetty, R.; Kundu, S.; Xia, W.; Bron, M.; Schuhmann, W.; Chirila, V.; Brandl, W.; Reinecke, T.; Muhler, M. PtRu Nanoparticles Supported on Nitrogen-Doped Multiwalled Carbon Nanotubes as Catalyst for Methanol Electrooxidation. *Electrochim. Acta* **2009**, *54*, 4208–4215.